Journal of Molecular Graphics and Modelling 29 (2010) 538–545

Contents lists available at ScienceDirect

Journal of Molecular Graphics and Modelling

journal homepage: www.elsevier.com/locate/JMGM

Binding research on flavones as ligands of β-amyloid aggregates by fluorescence and their 3D-QSAR, docking studies

Yang Yang, Lin Zhu, Xiangji Chen, Huabei Zhang*

Key Laboratory of Radiopharmaceuticals, Ministry of Education, College of Chemistry, Beijing Normal University, Beijing 100875, PR China

ARTICLE INFO

Article history:
Received 3 May 2010
Received in revised form 15 October 2010
Accepted 18 October 2010
Available online 23 October 2010

Keywords:
Alzheimer's disease
$A\beta_{(1-40)}$ aggregates
Flavone derivatives
Fluorescence
K_d
CoMSIA
AutoDock

ABSTRACT

The K_ds (dissociation constants) of 21 flavone derivatives have been obtained by fluorescence in vitro when binding with $A\beta_{(1-40)}$ (β-amyloid$_{(1-40)}$) aggregates protein. Extensive 3D-QSAR (quantitative structure–activity relationship) studies were performed on the fluorescent flavones, which are excellent ligands of $A\beta_{(1-40)}$ aggregates protein. Comparative molecular similarity indices analysis (CoMSIA) technique was used to relate the binding affinities with the ligand structures, and the QSAR model was obtained using the CoMFA technique. The QSAR model was proved to statistically significant and have high predictive power: the CoMSIA model yielded the cross-validated $q^2 = 0.512$ and the non-cross-validated $r^2 = 0.911$. This model showed that electrostatic (22.5%) and H-bond interaction (acceptor 15.3%; donor 45.1%) properties played major roles in ligand binding process. The QSAR model was further graphically interpreted in terms of field contribution maps. In order to further investigate the specific binding site of the flavones in the $A\beta_{(1-40)}$ aggregates, preliminary docking studies were performed. According to the 3D-QSAR results, the possible binding site in the protein was proposed in order to direct the molecular docking studies. A good correlation (R^2: 0.846) between the calculated binding energies and the experimental binding affinities (pK_ds) suggests that the identified binding site is reliable. The 3D-QSAR model and the information of the ligand–protein interaction will be helpful in the selection of flavones to be structurally modified and labeled by a radio nuclide for imaging $A\beta_{(1-40)}$ aggregates in the AD (Alzheimer's disease) brain.

1. Introduction

Alzheimer's disease (AD) is characterized by both abundant senile plaques (SPs) and numerous neurofibrillary tangles (NFTs) in the brain, while the SPs were composed of β-amyloid (Aβ) peptides and the NFTs were formed by filaments of highly phosphorylated tau proteins. However, early appraisal of AD is currently based on the clinical observation of cognitive decline, which is often unreliable and coupled with the systematic elimination of other possible causes [1–4]. The only definitive confirmation of AD is dependent on only postmortem histopathological examination of Aβ deposits in the brain by fluorescent Thioflavin T or Congo Red. Therefore, in vivo non-invasive imaging of β-amyloid plaques in the living brain would be necessary for early detection of AD [5,6], and many radio-labeled biomarkers for direct mapping β-amyloid plaques by SPECT and PET have been reported [7–15]. Currently, radio-iodinated and radio-fluorided flavone derivatives have been undertaken to develop novel probes for targeting Aβ plaques by Ono et al. [16,17], the corresponding biological evaluation (radioautography and biodistribution) results, in addition of the hypotoxicity of the flavone derivatives, suggested that efforts should focused on the development of diagnostic flavone derivatives labeled by isotopes of ^{99m}Tc, ^{123}I, ^{18}F, or ^{11}C as candidates for the plaques imaging. However, it takes on a lot of sophisticated experiments to obtain the final and ideal radio-tracers usually, thus in order to select several flavones rapidly and efficiently for radiolabelling and biological evaluation, we sought to elucidate the relationship between the concentrations of the ligands and fluorescence intensities by in vitro measuring the K_ds that could be used to evaluate the binding affinities when these flavones binding with $A\beta_{(1-40)}$ aggregates protein, which was often used as an in vitro model of the β-amyloid plaques. The similar measurement method by fluorescence was according to H. Levine-III's research [18]. Furthermore, there was no report on the binding sites of flavone-$A\beta_{(1-40)}$ aggregates protein complex, the obtained K_ds may be helpful in the theoretic prediction of the "pocket" & interaction mechanism.

Here, we obtained all the K_ds of 21 flavones when binding with $A\beta_{(1-40)}$ aggregates protein by fluorescence, and performed 3D-QSAR analysis and preliminary molecular docking studies to investigate the possible binding site in the protein, and our research

* Corresponding author. Tel.: +86 10 58802961.
E-mail address: hbzhang@bnu.edu.cn (H. Zhang).

1093-3263/$ – see front matter © 2010 Elsevier Inc. All rights reserved.
doi:10.1016/j.jmgm.2010.10.006

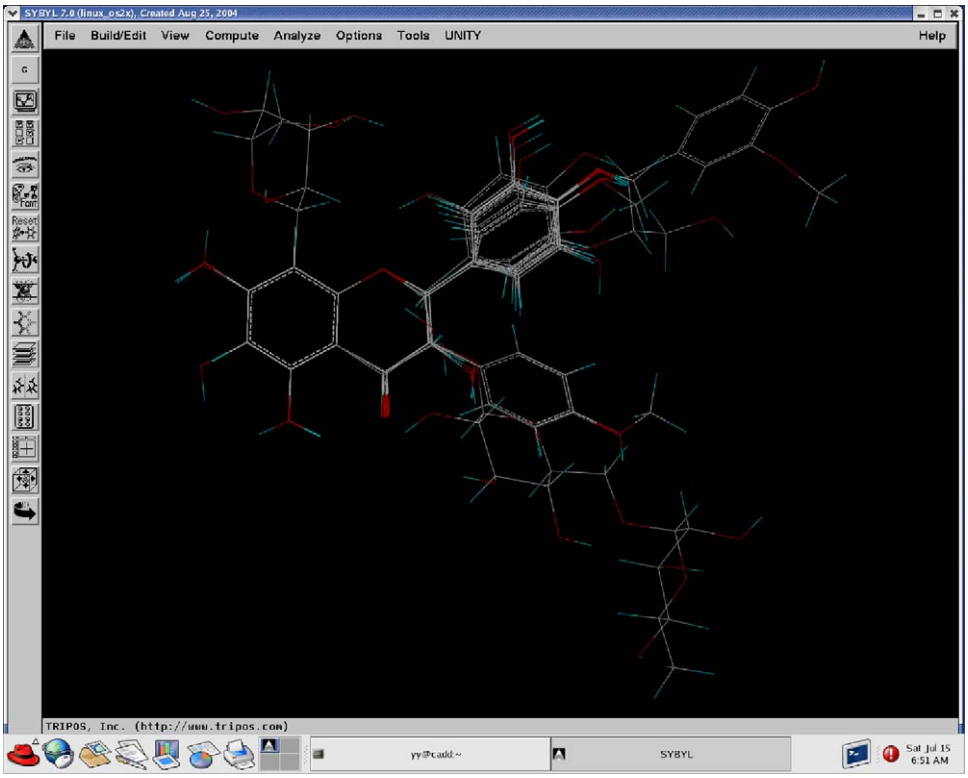

Fig. 1. Structural optimization of flavone derivatives by SYBYL7.0.

could also contribute to design and prepare new Aβ imaging agents based on the molecular skeleton of the flavones.

2. Materials

$A\beta_{(1-40)}$ peptide was purchased from Shang Hai "Supermed" Co., Ltd. Thioflavin T and PBS (phosphate buffer solution, pH 7.4) were purchased from Sigma–Aldrich Chemical Company. Flavone derivatives were purchased from Alfa Aesar China (Tianjin) Co., Ltd., Chinese CRM/RM Information Center, and obtained from the research groups of Prof. Mei Han, associate Prof. Xi Yan and Prof. Mengxia Xie, respectively. Other chemicals were all purchased from Beijing Chemical Reagents Company without further purification.

3. Experiments

3.1. Pre-formed synthetic $A\beta_{(1-40)}$ aggregates

$A\beta_{(1-40)}$ aggregates were prepared according to the method published previously [19]. 0.9 mg $A\beta_{(1-40)}$ peptide was dissolved in 2 mL PBS to form a final concentration of 450 μg/mL (100 μM). This solution was stirred at 350 rpm for 72 h at room temperature until the solution was visibly cloudy.

3.2. Binding assays in vitro by fluorescence spectroscopy

According to the similar method published [18], 21 K_ds of flavones when binding with $A\beta_{(1-40)}$ aggregates in PBS solution were all obtained by fluorescence spectroscopy. For example (flavone-001): fresh solution of flavone-001 was diluted to obtain a final concentration range of 8–24 nM. 5 μL solution of $A\beta_{(1-40)}$ aggregates was added to each PBS solution (500 μL) of the flavone-001, respectively, then these mixed solutions were all incubated for 1 min at room temperature before measuring the fluorescence intensities. Excitation wavelength was 320 nm (slit-width: 2 nm) and a scan range of 430–700 nm was performed. All the data were measured for three times. The linear relationship between the concentrations and the fluorescence intensities was analyzed by "double reciprocal plot".

4. Computational methods

4.1. Molecular modeling

All modeling works were performed using Sybyl 7.0 software package [20]. The initial geometry of each compound was optimized using standard Tripos Force Field loaded gasteiger-huckel charge using conjugated gradient method with an energy convergence criterion of 0.01 kcal/mol, followed by a systematic search for the structure (for rotatable bonds, the 10° increments from 0° to 360° were used). All the structures of flavone derivatives were fully optimized and the partial atomic charges required for electrostatic interaction were computed by semi-empirical molecular orbital methods based on MOPAC with AM1 Hamiltonian (key word: NOMM); the lowest energy structures were used in alignment. All the flavone derivatives are highlighted and shown in Fig. 1 and Table 1.

4.2. 3D-QSAR (CoMSIA)

CoMSIA studies were performed on the original data of 21 flavones. The dependent variable was defined as the inverse log of the K_d value. The relationship between binding affinities, expressed as the pK_ds ($-\log K_d$s), and a series of molecular descriptors was quantitatively studied by the means of partial least-squares analysis (PLS). Five physicochemical properties (steric, electrostatic, hydrophobic fields, and hydrogen bond donor and acceptor) were evaluated. All CoMSIA calculations were performed using SYBYL

Table 1
The structure and in vitro binding affinities of the 21 flavones.

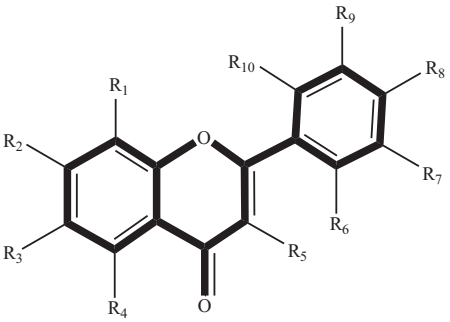

A

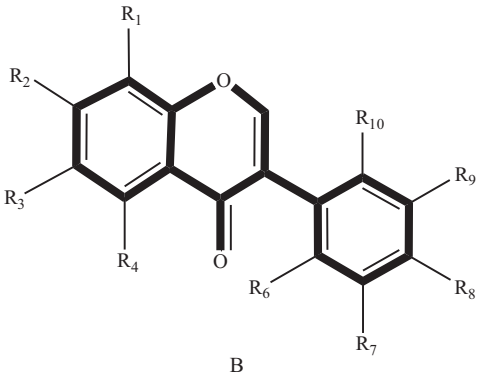

B

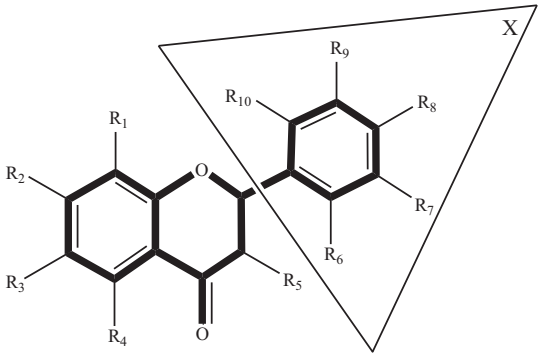

C

.

No.		R_1	R_2	R_3	R_4	R_5	R_6	R_7	R_8	R_9	R_{10}	K_d (nM)	pK_d
002		H	H	H	H	OH	H	H	H	H	H	301.93	6.52
003		H	OH	H	OH	Z	H	H	OH	OH	H	390.95	6.41
004		H	OH	H	OH	OH	H	H	OH	OH	H	2.40	8.62
005		H	OH	H	OH	H	H	H	H	H	H	58.07	7.24
006	A	H	H	H	H	H	H	H	H	H	H	31.78	7.50
007		H	OH	H	OH	OH	H	H	OH	H	OH	48.04	7.32
008		H	OH	H	OH	H	H	H	OH	H	H	55.33	7.26
009		H	OH	H	H	OH	H	H	OH	OH	H	3.61	8.44
010		H	OH	H	OH	OH	H	OH	OH	OH	H	18.23	7.74
011		H	OH	OH	OH	H	H	H	H	H	H	61.17	7.21
016		H	OH	H	OH	H	H	H	OH	OH	H	3.80	8.42
017		H	OH	H	OH	OH	H	H	OH	H	H	326.81	6.49
019	B	H	OH	H	OH	H	H	H	OCH_3	OH	H	8.02	8.10
001		H	OH	H	H	–	H	H	OH	H	H	60.68	7.22
014		H	OH	H	OH	–	H	H	OH	H	H	7.63	8.18
018		H	OH	H	H	–	H	H	OH	H	H	30.65	7.51
021		Y	OH	H	H	–	H	H	OH	H	H	45.05	7.35
012		H	OH	H	OH	OH	H	H	OH	H	H	32.12	7.49
013	C	H	OH	H	OH	OH	H	H	OCH_3	OH	H	210.52	6.68
015		H	OH	H	OH	H	H	H	OH	H	H	7.04	8.15
020		H	OH	H	OH	OH (S)			X			240.74	6.62

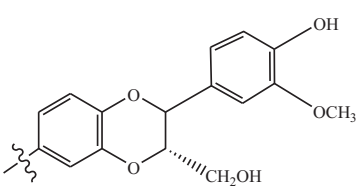

X

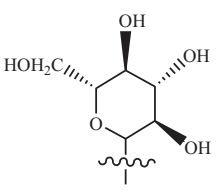

Y

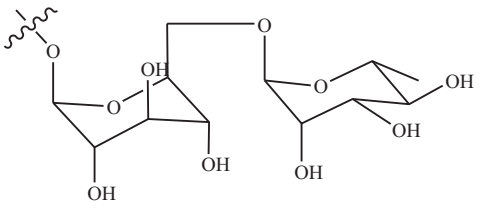

Z

7.0, and the standard settings (sp^3-carbon probe atom with charge +1, VDW radius 1 Å, grid spacing 2 Å, and 0.3 as attenuation factor α for the distance) were used. PLS methodology was used to correlate flavones with the CoMSIA values. Column filtering value (σ) was set to 2.0 kcal/mol to improve the signal-to-noise ratio. The predictive value of the models was evaluated by leave-one-out (LOO) cross-validation. The optimum number of components (ONC) corresponding to the lowest PRESS value was used for deriving the final PLS regression models. In addition to the ONC, the non-cross-validated (r^2), cross-validated (q^2), standard error of estimate (SE) and *F*-ratio (*F*) were also computed.

4.3. Molecular docking

The $A\beta_{(1-40)}$ aggregates structure (Fig. 2) composed of five repeated β-strands generated by Petkova et al. [21] was chosen

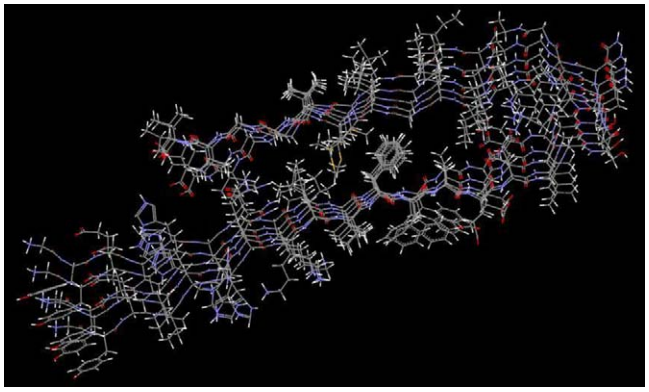

Fig. 2. The 3D-structure of $A_{(1-40)}$ aggregates.

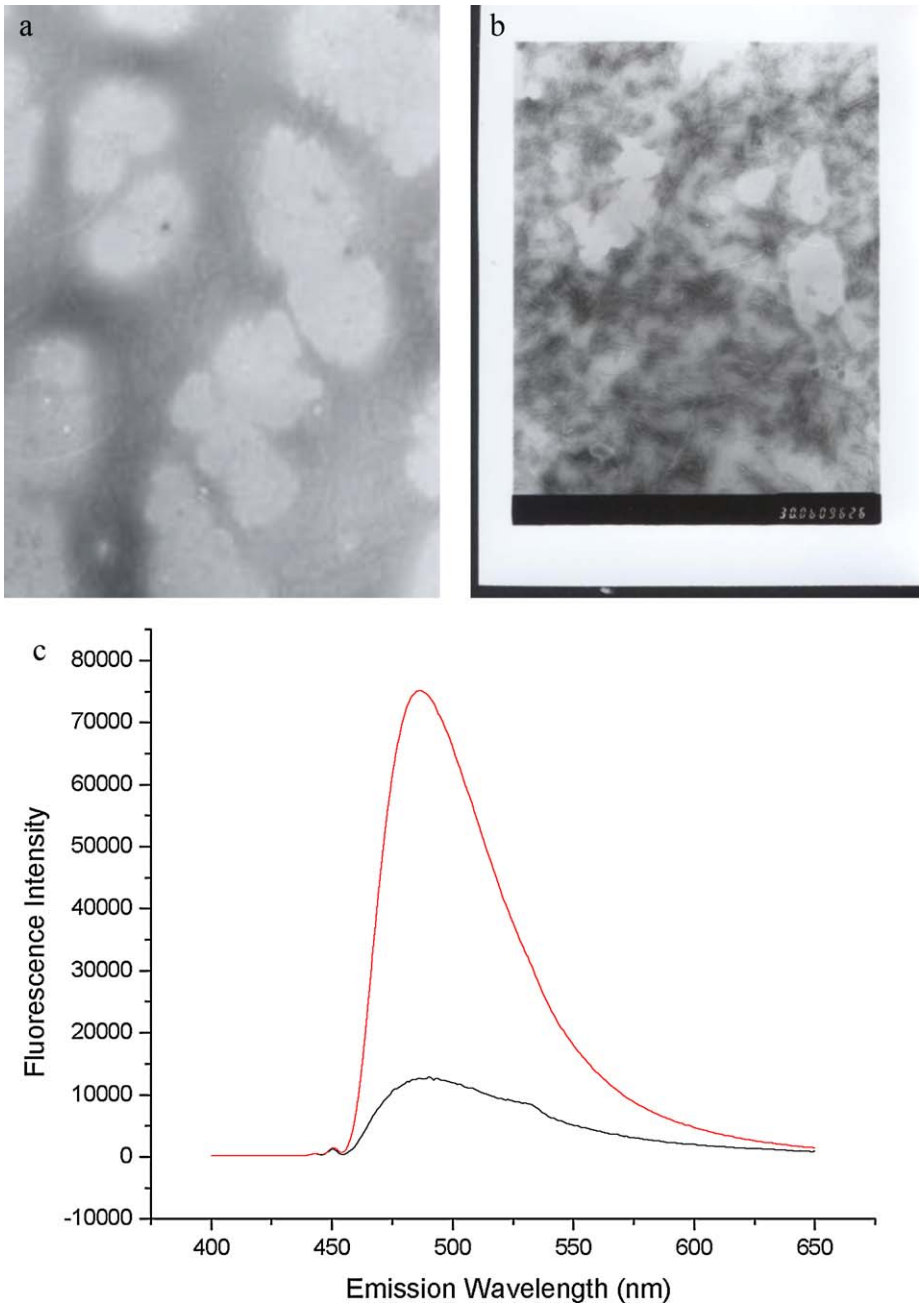

Fig. 3. Observation of $A\beta_{(1-40)}$ peptide (a) and $A\beta_{(1-40)}$ aggregates (b) by transmission electron microscope. Proof of the formation of $A\beta_{(1-40)}$ aggregates by Thioflavine T (c).

as the macromolecule model. Based on the results of 3D-QSAR of the original 21 flavone derivatives, a possible binding site in $A\beta_{(1-40)}$ aggregates molecule was proposed. Three flavone derivatives (No. 013, 001 and 017) with low binding affinities, three ligands (No. 005, 006 and 011) with mediate binding affinities and three ligands (No. 009, 014 and 016) with high binding affinities were randomly selected in docking studies to validate this proposal. A systemic search for binding site demonstrated the flavones entered a channel of five repeated β-strands formed by PHE-11 and ILE-23 and residues along its long axis, and this channel was applied for Grid program, followed by automatical docking studies using AutoDock 4.0. In addition, the Lamarckian Genetic Algorithm (LGA) was applied to deal with the ligand–protein interactions.

The whole docking operation could be stated as follows: first, the $A\beta_{(1-40)}$ aggregates was checked for polar hydrogen and assigned for partial atomic charges; and a PDBQT file was then created. Atomic salvation parameters and fragmental volumes were assigned to the $A\beta_{(1-40)}$ aggregates using "ADDSOL" module of the AutoDock program. Meanwhile, some of the torsion angles of the ligands were defined, allowing the conformation search for the ligands during the docking process. Secondly, the grid map with $50 \times 50 \times 50$ and a spacing of 0.375 Å was calculated using the 'AutoGrid' module to evaluate the binding energies between the ligands and the $A\beta_{(1-40)}$ aggregates. The affinity and electrostatics potential grid were calculated for each type of atom in the flavone and the energy configuration of a particular ligand was found by tri-linear interpolation of affinity values around each atom. Third, some important parameters for LGA calculations were reasonably set up according to requirements of the Amber force field and our target. The mutation rate was 0.02 which was a probability that a gene would undergo a random change. The maximum number of generations and energy evaluations were both 5.0×10^5. The crossover rate, which was the probability of proportional selection, was set to 0.8. Quaternion step and Torsion step was set to 10°. All active bonds were set rotatable. All docked compounds were subjected to 250 runs of hybrid GA-LS search. Each run was composed of 4000 iterations of soils and wets local search. The final data taken from docking experiments produced the lowest total docked energy. Finally, the docked complexes of the ligand–protein for each ligand were selected according to the criterion of interaction energy combined with geometrical matching quality. The hydrophobicity of this area was detected using DRY probe in grid program.

4.4. Binding free energy prediction

Binding free energy prediction was computed in AutoDock 4.0 [22] to evaluate the binding affinities between the protein and the ligands and the new scoring function was developed based on the traditional molecular force field model of interaction energy. The total binding free energy was estimated based on the above-stated terms and a set of coefficient factors (the restriction of internal rotors, the global rotation, and the translation were modeled depending on the number of torsion angles of the ligand and the desolvation upon binding and the hydrophobic effect were calculated).

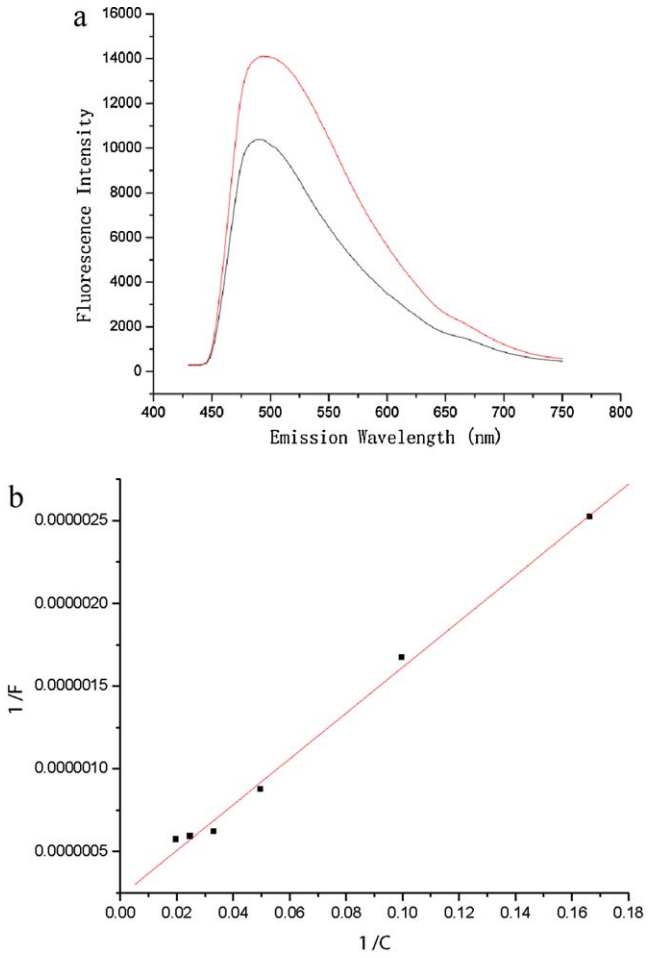

Fig. 4. (a) Black line represents flavone-001 and red line represents flavone-001 binding to $A\beta_{(1-40)}$ aggregates; (b) "double reciprocal plot". (For interpretation of the references to color in this figure legend, the reader is referred to the web version of the article.)

5. Results and discussions

5.1. Pre-formed synthetic $A\beta_{(1-40)}$ aggregates

$A\beta_{(1-40)}$ aggregates were prepared successfully, because the formation of $A\beta_{(1-40)}$ aggregates was proved by transmission electron microscope, in comparison to $A\beta_{(1-40)}$ peptide (Fig. 3). The formation of $A\beta_{(1-40)}$ aggregates was also identified by Thioflavine T (8 μM) [18].

5.2. Binding assays in vitro by fluorescence spectroscopy

There was an obvious enhance of fluorescence intensity of flavone-001 (8 nM, 500 μL) when 5 μL $A\beta_{(1-40)}$ aggregates was added to the same solution of flavone-001 (Fig. 4a). The linear relationship between the concentrations of flavone-001 (incubated with $A\beta_{(1-40)}$ aggregates) and fluorescence intensities was analyzed by "double reciprocal plot", and the results were shown in

Table 2
CoMSIA results of flavones.

ONC	q^2	r^2	SE	F	Field contribution				
					Steric	Electrostatic	Hydrophobic	Donor	Acceptor
6	0.512	0.911	0.236	224.015	0.052	0.225	0.119	0.451	0.153

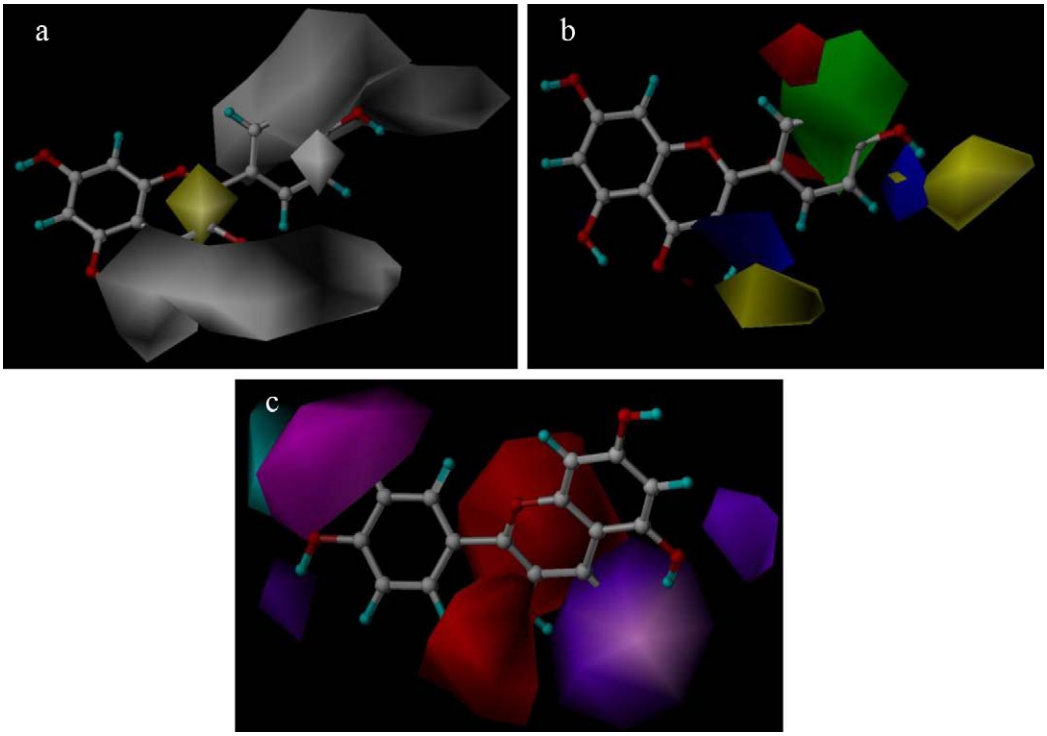

Fig. 5. CoMSIA contour maps based on docking alignment method. Hydrophobic favored areas (contribution level of 90%) in yellow, hydrophobic unfavored areas (contribution level of 10%) in white. Positive-charge-favored areas (contribution level of 80%) in blue, positive-charge-unfavored areas (contribution level of 20%) in red. Sterically favored areas (contribution level of 80%) in green, sterically unfavored areas (contribution level of 20%) in yellow. Donor-favored areas (contribution level of 80%) in cyan, donor-unfavored areas (contribution level of 20%) in purple. Acceptor favored areas (contribution level of 80%) in magenta, acceptor unfavored areas (contribution level of 20%) in red. (a) Hydrophobic contour maps; (b) positive-charge and steric contour maps; (c) donor and acceptor contour maps. (For interpretation of the references to color in this figure legend, the reader is referred to the web version of the article.)

Eq. (1) and Fig. 4b.

$$Y = 2.28152E-7 + 1.38433E-5X \quad R^2: 0.99507,$$
$$\text{SD}: 6.23724E-8, \quad P < 0.0001, \quad F: 808.61387 \qquad (1)$$

where Y is $1/F$(1/fluorescence intensity), X is $1/C$(1/concentration (nM)), R^2 is linear correlation coefficient, SD is standard deviation.

$$K_d = \frac{1.38433E-5}{2.28152E-7} = 60.68\,\text{nM}, \quad \text{p}K_d = -\log K_d = 7.22$$

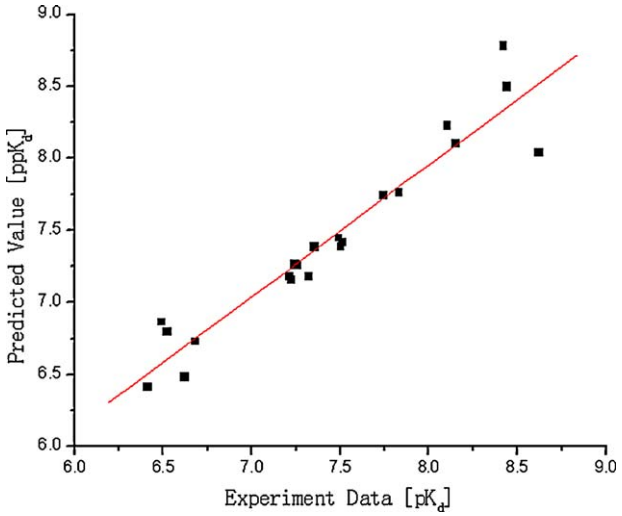

Fig. 6. The ppK_d versus pK_d based on the CoMSIA model.

Therefore, all the K_ds of flavones were obtained according to the same method to that of flavone-001 (Table 1).

5.3. Graphics interpretation of QSAR models

CoMSIA analysis of flavones showed the cross-validated $q^2 = 0.512$ and the non-cross-validated $r^2 = 0.911$. The comparison of the predictive index of 3D-QSAR models for the test set was shown in Table 2. The contour maps for fields that were included in the CoMSIA model were shown in Fig. 5(a–c) with compound flavone-004 as the reference structure.

Fig. 5a shows the hydrophobic contour maps. The large white regions indicated that the hydrophilic substitution in position of R_5, R_8 and R_9, and the hydrophobic substitution in position of C=C bond.

Fig. 5b shows the positive-charge and Steric contour maps. The green region on position of R_8 and R_9 indicated that and bulky substitution was favored here, whereas a yellow area around R_5 and R_7 substitutions indicated a sterically disfavored region. The blue region on position of R_4, R_5, R_7 and R_8 indicated that the positive-charge group was favored here, while a red area presented at the position of R_6 and R_9 indicated that a positive-charge group was unfavored.

Fig. 5c shows hydrogen-bond donor and acceptor contour maps. The cyan region on position of R_8 indicated that a donor was favored here, whereas a purple area around R_9 substitutions indicated a donor disfavored region. The magenta region of R_3, R_4, R_7 and C=O indicated an acceptor favored region, but the red region around R_5 and –C=C–O group is presented acceptor disfavored.

Fig. 6 shows the predicted binding affinities (ppK_d) versus experimental binding affinities (pK_d) by the CoMSIA model. The data was fit linear, and there was a good linear relationship between

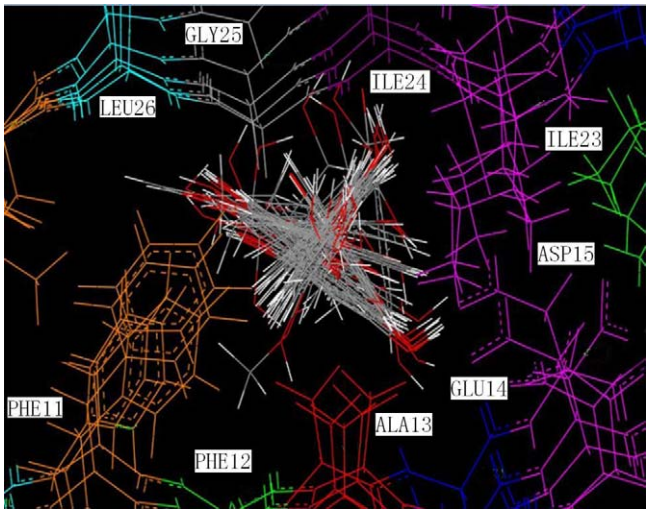

Fig. 7. The binding conformations of the flavone derivatives displayed inside the channel of $A\beta_{(1-40)}$ aggregates.

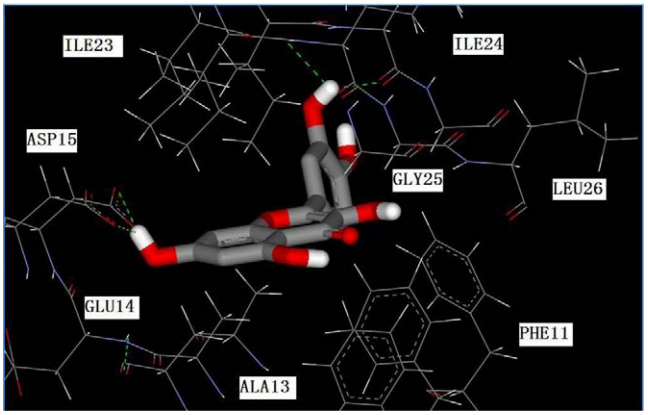

Fig. 8. Key residues of the binding site of flavone-004 is presented in green sticks. (For interpretation of the references to color in this figure legend, the reader is referred to the web version of the article.)

ppK_d and pK_d (Eq. (2)), which demonstrated that the CoMSIA model would be credible.

$$Y = 0.65817 + 0.91146X \quad R^2: \quad 0.91134, \quad \text{SD}: \quad 0.1935,$$

$$F\text{-value}: \quad 195.27805 \qquad (2)$$

where Y is predicted value [ppK_d] and X is experiment data [pK_d]; SD is standard error and R^2 is correlation coefficient.

It was found that the obtained q^2 (0.512) was much lower than the correlation coefficient r^2 (0.911), which indicated that overfitting happened within the CoMSIA approaches. In our opinion, the reason why q^2 was much lower than r^2 was that CoMSIA model could not predict pK_ds of several molecules very well, especially compound 004 and 016. There are five –OH groups on the positions of R_2, R_4, R_5, R_8, and R_9 and four –OH groups on the positions of R_2, R_4, R_8, and R_9 in the structures of compound 004 and 016, respectively. According to the CoMSIA model, area around R_9 substitutions indicated a donor-disfavored region, which showed –OH was disfavored, moreover, hydrophilic substitution should be in position of R_5, R_8 and R_9, but compound 016 has only =CH– group in position of R_5; positive-charge should be around R_5, but –OH was a negative-charge group; as a result, differences between experimental and corresponding predicted pK_ds of compound 004 and 016 were bigger than that of other compounds. The CoMSIA could not explain why compound 004 and 016 indicated high binding affinities with β-amyloid aggregates completely so that q^2 is lower than r^2.

According to the obtained CoMSIA model here, β-amyloid aggregates imaging agents can be designed as: hydrophilic, acceptor favored, and small group should be introduced into position R_8, and the candidates are –OH, $–NH_2$, $–NHCH_3$; donor-unfavored groups should be introduced into position R_3 such as –CH= or radio Tc–, I–, F–, and $F(CH_2)_nO–$; hydrophobic group in position of C=C bond was favored; in addition, in order to increase the penetration of imaging agents into BBB (blood–brain barrier), –OH on other positions might be deleted. Fortunately, the designed imaging agents here agreed with I-125 and F-18 labeled compounds reported by Ono et al. [16,17] very well, the I-125 labeled flavones showed 22.6–72.5 nM of K_i values and the F-18 labeled flavones showed 5.3–321.1 nM of K_i values, respectively, which demonstrated high binding affinities of these complexes with β-amyloid aggregates, and that means the CoMSIA model established by our research group can be applied for design of agents for imaging β-amyloid aggregates in the future.

5.4. Molecular docking studies of the ligands and binding conformation

A hydrophobic channel was found in the amyloid protein using DRY probe in grid. Analysis of results from AutoDock 4.0 revealed that all the flavone series entered the hydrophobic channel with the long axis parallel to the long axis of protein as depiction in Figs. 7 and 8 and the aromatic moieties of the flavones were parallel with PHE-11 residues. These parallel orientations of aromatic rings were the most common orientation for π–π stacking and this binding model could favor electron transfer between ligand and protein. As the flavones wholly entered the hydrophobic channel with their long axises parallel to the long axis of protein, we speculated that introduction of some bulky groups in the middle of molecule would decrease their activities dramatically because it would hinder the ligand molecule from entering the hydrophobic channel, and this hypothesis above has been proved by that flavone-003, 020 and 021 (6.41, 6.62, 7.35) showed low binding affinities because of bulky groups in their structures.

5.5. Correlation between binding free energy and experimental binding affinity

The predicted binding free energies (ΔGs) of ligands were listed in Table 3 and the correlation was found between ΔGs and the pK_ds (Eq. (3)) by linear regression analysis. The correlation coefficient (R^2) was 0.846, and the rather good correlation demonstrated that we had successfully discovered the most probable binding site.

$$\Delta G = -3.3944 - 0.4539\,\text{p}K_d \quad R^2: \quad 0.846, \quad \text{SD}: \quad 0.13397,$$

$$F\text{-value}: \quad 32.83505 \qquad (3)$$

where R^2 is correlation coefficient and SD is standard error.

Table 3
The experimental binding affinities (pK_d), predicted binding free energies (ΔG, kcal/mol, T = 298.15 K), number of torsional degrees of freedom (TD) and No. of conformations (NC) in the corresponding ranked cluster (cluster).

No.	pK_d	ΔG (kcal/mol)	TD	Cluster	NC
002	6.52	−6.37	2	2	4
001	7.22	−6.77	3	2	7
004	8.62	−7.44	6	2	24
005	7.24	−6.82	3	1	32
008	7.26	−6.69	7	2	8
015	8.15	−6.97	4	1	1
012	7.49	−6.58	3	1	32
021	7.35	−6.67	8	1	9

6. Conclusion

In conclusion, a series of novel flavones have been evaluated as probes for $A\beta_{(1-40)}$ aggregates by fluorescence, and the probable binding site between the flavones and the $A\beta_{(1-40)}$ aggregates was proposed. The 3D-QSAR model and the information of the ligand–protein interaction will be helpful in the selection of flavones to be structurally modified and labeled by a radio nuclide for imaging $A\beta_{(1-40)}$ aggregates in the AD brain.

Acknowledgements

We thank Prof. Robert Tycko (National Institutes of Health, USA) very much for his kindness in offering the $A\beta_{(1-40)}$ aggregates structure. We also thank Prof. Mei Han (College of Chemistry, Beijing Normal University, PRC), associate Prof. Xi Yan (College of Chemistry, Beijing Normal University, PRC) and Prof. Mengxia Xie (Analytical and Testing Center, Beijing Normal University, PRC) very much for their kindness in offering several flavones. This work was financially supported by the Natural Science Foundation of China (No. 20671013); National Basic Research Program of China (No. 2006CB500705).

References

[1] G. McKhann, D. Drachman, M. Folstein, R. Katzman, D. Price, E.M. Stadlan, Clinical diagnosis of Alzheimer's disease: report of the NINCDS-ADRDA work group under the auspices of the department of health and human services task force on Alzheimer's disease, Neurology 34 (1984) 939–944.
[2] M.F. Weiner, Alzheimer's disease: diagnosis and treatment, Harv. Rev. Psychiatry 4 (1997) 306–316.
[3] D.J. Selkoe, Amyloid beta-protein and the genetics of Alzheimer's disease, J. Biol. Chem. 271 (1996) 18295–18298.
[4] D.J. Selkoe, Alzheimer's disease: genes, proteins, and therapy, Physiol. Rev. 81 (2001) 741–766.
[5] C.A. Mathis, Y. Wang, W.E. Klunk, Imaging beta-amyloid plaques and neurofibrillary tangles in the aging human brain, Curr. Pharm. Des. 10 (2004) 1469–1492.
[6] A. Nordberg, PET imaging of amyloid in Alzheimer's disease, Lancet. Neurol. 3 (2004) 519–527.
[7] T.T. Ashburn, H. Han, B.F. McGuinness, P.T. Lansbury, Amyloid probes based on Congo Red distinguish between fibrils comprising different peptides, Chem. Biol. 3 (1996) 351–358.
[8] H. Han, C.G. Cho, P.T. Lansbury Jr., Technetium complexes for the quantitation of brain amyloid, J. Am. Chem. Soc. 118 (1996) 4506–4507.
[9] W. Zhang, S. Oya, M.P. Kung, C. Hou, D.L. Maier, H.F. Kung, F-18 polyethyleneglycol stilbenes as PET imaging agents targeting Aβ aggregates in the brain, Nucl. Med. Biol. 32 (2005) 799–809.
[10] W. Zhang, S. Oya, M.P. Kung, C. Hou, D.L. Maier, H.F. Kung, F-18 stilbenes as PET imaging agents for detecting β-amyloid plaques in the brain, J. Med. Chem. 48 (2005) 5980–5988.
[11] W.E. Klunk, H. Engler, A. Nordberg, Y. Wang, G. Blomqvist, D.P. Holt, M. Bergstrom, I. Savitcheva, G.F. Huang, S. Estrada, B. Ausen, M.L. Debnath, J. Barletta, J.C. Price, J. Sandell, B.J. Lopresti, A. Wall, P. Koivisto, G. Antoni, C.A. Mathis, B. Langstrom, Imaging brain amyloid in Alzheimer's disease with Pittsburgh compound-B, Ann. Neurol. 55 (2004) 306–319.
[12] N.P. Verhoeff, A.A. Wilson, S. Takeshita, L. Trop, D. Hussey, K. Singh, H.F. Kung, M.P. Kung, S. Houle, In vivo imaging of Alzheimer disease beta-amyloid with [^{11}C]SB-13 PET, Am. J. Geriatr. Psychiatry 12 (2004) 584–595.
[13] N. Okamura, T. Suemoto, H. Shimadzu, M. Suzuki, T. Shiomitsu, H. Akatsu, T. Yamamoto, M. Staufenbiel, K. Yanai, H. Arai, H. Sasaki, Y. Kudo, T. Sawada, Styrylbenzoxazole derivatives for in vivo imaging of amyloid plaques in the brain, J. Neurosci. 24 (2004) 2535–2541.
[14] K. Shoghi-Jadid, G.W. Small, E.D. Agdeppa, V. Kepe, L.M. Ercoli, P. Siddarth, S. Read, N. Satyamurthy, A. Petric, S.C. Huang, J.R. Barrio, J. Liu, S. Flores-Torres, G.M. Cole, Localization of neurofibrillary tangles and beta-amyloid plaques in the brains of living patients with Alzheimer disease: binding characteristics of radiofluorinated 6-dialkylamino-2-naphthylethylidene derivatives as positron emission tomography imaging probes for beta-amyloid plaques in Alzheimer disease, Am. J. Geriatr. Psychiatry 10 (2002) 24–35.
[15] C.A. Mathis, Y. Wang, W.E. Klunk, Imaging β-amyloid plaques and neurofibrillary tangles in the aging human brain, Curr. Pharm. Des. 10 (2004) 1469–1492.
[16] M. Ono, N. Yoshida, K. Ishibashi, M. Haratake, Y. Arano, H. Mori, M. Nakayama, Radioiodinated flavones for in vivo imaging of β-amyloid plaques in the brain, J. Med. Chem. 48 (2005) 7253–7260.
[17] M. Ono, R. Watanabe, H. Kawashima, T. Kawai, H. Watanabe, M. Haratake, H. Saji, M. Nakayama, ^{18}F-labeled flavones for in vivo imaging of β-amyloid plaques in Alzheimer's brains, Bioorg. Med. Chem. 17 (2009) 2069–2076.
[18] H. Levine III, Thioflavine T interaction with synthetic Alzheimer's disease {beta}-amyloid peptides: detection of amyloid aggregation in solution, Protein Sci. 2 (1993) 404–410.
[19] W.E. Klunk, R.F. Jacob, R.P. Mason, Quantifying amyloid beta-peptide (Abeta) aggregation using the Congo red-Abeta (CR-abeta) spectrophotometric assay, Anal. Biochem. 266 (1999) 66–76.
[20] Sybyl Version 7.0, Tripos Inc., 1699 Hanley Road, St. Louis.
[21] A.T. Petkova, Y. Ishii, J.J. Balbach, O.N. Antzutkin, R.D. Leapman, F. Delaglio, R. Tycko, A structural model for Alzheimer's β-amyloid fibrils based on experimental constraints from solid state NMR, Proc. Natl. Acad. Sci. U.S.A. 99 (2002) 16742–16747.
[22] V. Sharma, K.K. Pattanaik, V. Jayprakash, A. Basu, N. Mishra, A utility script for automating and integrating AutoDock and other associated programs for virtual screening, Bioinformation 4 (2009) 84–86.